A Study of Monopile with Super Large Diameter in Layered Soils

Zhen Huang [1]* Meng Jiang [2]*

1. State Key Laboratory of Coastal and Offshore Engineering, Dalian University of Technology, Dalian, 116024, China
2. Deepwater Engineering Research Center, Dalian University of Technology, Dalian 116024, China

Abstract: With the development of ocean engineering, monopiles with a large diameter foundation have gradually replaced those with small diameter and been applied to more and more ocean structures. The responses of monopiles with small diameter under wind, wave, current and seismic loads have been extensively studied. However, not too much work on large-diameter monopile (>9 m) has been carried out. In this study, finite element method (FEM) is adopted to study a monopile with a diameter of 9 m, and the mechanical responses is presented. Besides the P-Y curves calculated by different ways are compared. It shows that the API specification is more conservative than the results from FEM, which indicates that the performance of the structure can be used more completely. Large deformation and stress zones are generated around the piles, and the soil rotates around the bottom of the pile.
Keywords: Super Large Diameter Monopile**;** Lateral Load; P-Y Curve; FEM Analysis; ABAQUS

1. Introduction

Monopile is the most widely used foundation type for offshore wind turbines (OWTs) at shallow water. Because of its simplicity of installation, economical and the widely proven success of buried piles in supporting offshore resources acquisition facility, this kind of foundation has been thoroughly studied. Monopile for OWTs is a long steel component, commonly 22 – 40 m long, 3 – 6 m in diameter[1], with certain flexibility, usually penetrated in soil to support the upper structure. Wind and wave loads are usually the most common and important environment loads for the design of offshore wind turbine structure. In addition, in some extreme environment conditions, ice load and seismic load are also needed to be considered. Therefore, with the development of the engineering practice and the accumulation of experience, it is vital to gradually study the responses of OWTs subjected to combined wind, wave and other load actions[2].

Wang and Zhao et al[3], investigated the dynamic responses of offshore wind turbine (OWT) supported on monopile foundation in clay subjected to wind, wave and earthquake actions. Several affecting factors, such as wind velocity, induction factor, wave period, peak ground acceleration, and soil parameters on the dynamic responses of the system were studied. Zheng and Li [4]studied the joint action of strong ci earthquakes and moderate sea conditions, and investigated the structural response in dry flume, low and high calm water levels, with and without regular or random waves. The results show that the overlook of the effect of wave action in seismic analysis will lead to an underestimation of structural response, especially when the monopile foundation is dynamically sensitive. Chen and Huang[5] studied the vulnerability of the monopile for the offshore structures during seismic events. In the study, an integrated 3-D numerical model is set up to investigate the dynamic behavior of monopile-seawater-seabed coupling system in the frequency domain. The seismic responses of the coupling system, such as hydrodynamic pressure of seawater, pore pressure in seabed, as well as acceleration amplitudes in pile and seabed, are discussed. Besides the mechanical design, the durability of construction is also considered. Caglar and Geoffrey[6] studied the design and implementation of a cathodic protection system for offshore steel monopiles., and compared the requirements for coated and uncoated structures and discussed the other factors that need to be taken into consideration. Klar and Osman [7] presented an energy approach for the prediction of non-linear foundation behavior. It was shown that the approach provides a fair estimation of the overall foundation response. Under large displacements the method degenerates into conventional upper-bound calculations. Jonkman et al [8] presented model dynamics of floating-platform supported and monopile-supported offshore turbines. Results showed that the hydrodynamic and elastic-foundation effects strongly influence the turbine modal dynamics.

Among all the studies, the lateral resistance of piles under soil-pile interaction is one of the key design considerations in

many civil engineering structures both in onshore and offshore environment. Wind, wave and earthquake create significant lateral loads on piles. The response of a pile under lateral load is governed by the interaction behavior of complex three-dimensional soil-pile interaction. Various approaches have been proposed in the past to analyze the laterally loaded pile. As the main focus of the present study is to investigate the response of a free-headed single steel pipe pile in sand under lateral load, some previous studies and calculation methods are presented in the next part.

However, a large number of studies only focus on the foundations with small diameter, interacting with soil in single layer. The existing research results are not appropriate for foundations with large diameter in multiple layers of soil. The purpose of this paper is to present a series of finite element analysis of a steel pipe pile with a large diameter in sand and clay layers subjected to lateral load. In this paper, a monopile with a diameter of 9 m in soil is studied. The soil is consisted of 6 layers of sand or clay, means it is hard to calculate with formula or specification (Figure 1). Therefore, a 3D finite element model is built to simulate the interaction between soil and pile. Mechanical responses will be revealed and discussed based on the model. Moreover, p-y curves results calculated by ABAQUS and PLAXIS are compared with API [9] calculation results.

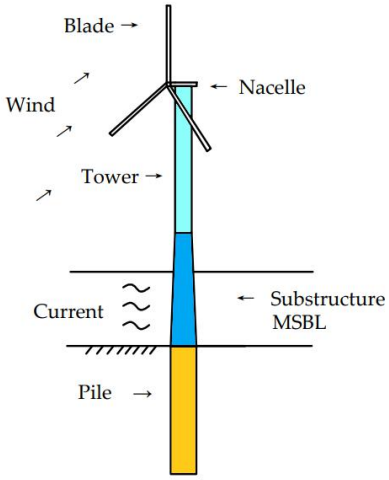

Figure 1. OWT model.

2. Methodology

Marine structures are subjected to loads induced from wind, wave, current and other environmental loads. The foundation of the structure interacts with the soil. The lateral deflection of pile head is strictly controlled in current design practice, especially in limit state design. The mechanical properties of soil are complicated, the interaction between pile and soil is always a focus in engineering practice and study. The failure of the pile-soil system is affected by the material, physical dimension and constraint condition. When the length of the pile is short and the head is free, the failure is subjected to the shear strength of the pile and the resistance of the soil. For long piles, the failure is subjected to the maximum bending moment and the resistance of the pile. So, the lateral resistance of the soil interacting with the pile is the focus of the academic research for a long time.

Several methods are used to study the lateral load deflection behavior of piles with soil: *m*-method, P-Y curve method, Apparent Fixity Length method (AFL method), coupled spring method and FEM.

2.1. *m*-method

In the *m*-method, the soil is assumed as linear elastic, ignoring the plasticity of soil. Therefore, it performs well with small deflection of pile, and it's gradually unsuitable with the increase of the load. However, as a simple and convenient method, it is written into the recommended practice and widely used for the pile-soil interaction analysis. The interaction force between the pile and soil is assumed to be in direct ratio to the pile-displacement. The proportional coefficient m of the lateral resistance coefficient of foundation soils is linear growth with the depth. The m is considered to be a fixed value but in

fact it's decreased with the increasing of load. It's applicable only in elastic stage in which the plasticity of the soil is ignored. However, as a simplified and convenient method, it is written into the recommended practice for the pile-soil interaction analysis. The modulus of soil reaction is as follows:

$$K_s = \mathrm{m} \cdot B_0 \cdot Z \tag{1}$$

where, m (kN/m^4) is the proportional coefficient of the horizontal resistance coefficient of foundation soils[10]; B_0 (m) is the calculative width of pile, and Z is the depth.

2. 2. P-Y curve method

In 1956, Mcclelland and Focht proposed p-y curve method to calculated nonlinear lateral resistance. Matlock proposed a method to define p-y curves in soft clay. Then Reese and O'Neill proposed method to define p-y curves in hard clay and sandy soil. The above three curves had been included in API specifications.

P-Y curve method is modified based on the Winkler foundation theory. A series of independent nonlinear springs are modeled to describe the soil (Figure 2). Because of the consideration of the spring nonlinearity, the curve can describe the non-linear or plasticity of soil. Theoretically, it is more accurate and suitable than m-method for offshore project[11]. The formula of soil reaction is as follows,

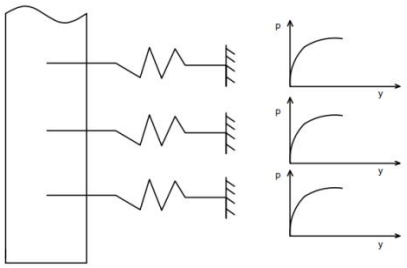

Figure 2. P-Y curve model.

For soft clay, the formula is defined in API specification as (2), where P_u is the ultimate reaction force of the soil. D is the diameter of the pile, Z is the depth, J is a constant of 0.25 ~ 0.5, Cu is the undrained shear strength, and ZR is the critical depth when the strength starts to decrease which can be calculated by (3). Where γ is the effective unit weight of the soil?

$$p_u = \begin{cases} C_u + \gamma Z + J\dfrac{C_u Z}{D} & 0 \le Z < Z_R \\ 9C_u & Z \ge Z_R \end{cases} \tag{2}$$

$$Z_R = \frac{6D}{J + \gamma D / C_u} \tag{3}$$

With p_u, p-y curve can be calculated by (4) and (5), where ε_{50} is the strain when the stress is the half of the maximum stress.

$$\frac{p}{p_u} = 0.5\left(\frac{y}{y_{50}}\right)^{1/3} \tag{4}$$

$$y_{50} = 2.5\varepsilon_{50} D \tag{5}$$

For hard clay which $C_u \geq 96$ kpa, Reese proposed the formula in (6).

$$p_u = \begin{cases} \left(2 + \frac{\gamma Z}{C_u} + \frac{2.83Z}{D}\right) \cdot C_u \cdot D \\ 11 C_u D \end{cases} \quad (6)$$

For shallow sand, the formula is defined in API specification with (7), and the coefficient for deeper soils can be obtained by (8)

$$P_u = (C_1 \cdot H + C_2 \cdot D)\gamma \cdot H \quad (7)$$

$$p_u = C_3 \cdot D \cdot \gamma \cdot H \quad (8)$$

where C_1, C_2, C_3 are parameters about the soil, γ is the effective unit weight of the soil, D is the diameter of the pile and H is a certain depth of the soil. With the p_u from the (7) and (8), the p-y curve can be calculated by (9):

$$p = A \cdot p_u \cdot \tanh\left(\frac{k \cdot H \cdot y}{A \cdot p_u}\right) \quad (9)$$

where A is the correction factor considering cyclic load or dead load, k is the initial foundation reaction modulus. A can be calculated by (10):

$$A = (3 - 0.8\frac{H}{D}) \geq 0.9 \quad (10)$$

2.3. AFL method

The AFL method is relatively simple, which is generally adopted to simplify the pile-soil interaction. It simulates a pile in the soil with an equivalent pile fixed in rigid foundation pile. The length of the pile ensures that the actual pile-soil stiffness coupling system has the same features to the model (Figure 3). Because of the nonlinear characteristics of soil, the stiffness of the soil should be a function of the load. This method is only applied well on a small scale with high accuracy. Cantilever beam is substituted for the pile for the AFL method.

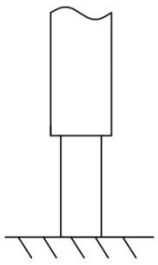

Figure 3. AFL method.

2.4. Coupled spring method

This method simulates the stiffness of a pile inserted into the seabed with two interrelated springs to describe the soil-pile interaction (Figure 4).

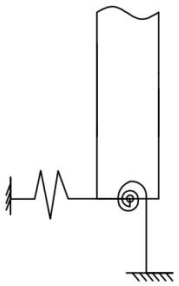

Figure 4. Coupled spring model.

2.5. Finite element method

In the FEM, the structure is modeled as continuum, which is presented by Poulos in a single pile-ideal elastic soil model in 1971.Then FEM is accepted and used widely by researchers. Kourkoulis et al[12] investigated the response of wind turbines founded on suction caissons and subjected to wave and earthquake loading using non-linear three-dimensional finite-element analyses. G Cao et al[13] carried out the component analysis of OWTs subjected to soil, wave and wind load. The difference of the dynamic responses between the OWT model with traditional p-y method and the new model is compared based on 3D finite element method. The numerical analysis shows that traditional p-y method overestimates the top displacements of OWT under stochastic wind and wave loads.

3. Numerical modelling

In this paper, ABAQUS is used to model the soil-pile interaction system for finite element analysis. Compared with other softwares, ABAQUS has the advantage of high accuracy in calculating soil nonlinearity. Therefore, it is widely used in the analysis of pile-soil interaction. In addition, ABAQUS has a good post-processing function, which can intuitively display the deformation and stress nephogram of pile and soil. As the model is presented in Figure 5, the pile is modeled as a solid pile with an equivalent stiffness. The equivalent stiffness is calculated as the ratio of the bending stiffness for a hallow pile and a solid pile, assuming a steel Young's modulus of 210 GPa. It is modeled as a linear elastic material with an equivalent stiffness, E', of 19.79 GPa and a Poisson's ratio, ν, of 0.3. The diameter of the pile is 9m, and the length is 45 m. The soil domain is created with 189m diameter(from -10.5*D to 10.5*D) and 90 m depth, The steel pile is located in the center of soil domain, completely buried in the earth. The size of soil domain is large enough to ignore boundary effects. All degrees of freedom are restrained in the bottom of soil, while the curved face of the soil domain is restrained from any radical displacement, and the top is free. The parameters used for pile is shown in Table 1.

Both soil and pile are modeled using the solid homogeneous C3D8R elements, which are 8-noded linear brick element with reduced integration and hourglass control. This kind of element is more applicable to interaction analysis, with a higher accuracy of displacement results, and will not create shear locking problem

.

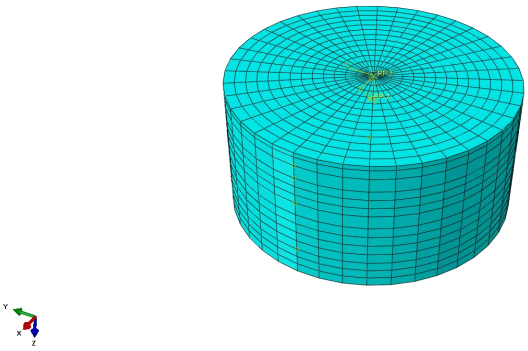

Figure 5. Finite element model.

3.1. Model of soil

The soil is consisted of sand layer and clay layer, which is simulated with Mohr- Coulomb theory. The soil has an effective unit weight, γ', of 10 kN/m3. The stiffness and strength properties of the sand layer have been decided based on correlations in literature[14] and shown in Table 2.

For clay layers in Abaqus analyses, the Mohr-Coulomb model is utilized. By specifying 0° friction angle and 0°dilation angle, it reduces to the pressure-independent Tresca model. A Poisson's ratio υ of 0.48 was used to simulate undrained conditions. An elastic modulus E is specified which remains constant in each layer to calculate the elastic deformation over the entire stress range. The equivalent elastic shear modulus G can therefore be calculated by:

$$G = \frac{E}{2(1+\nu)} \tag{11}$$

For undrained conditions, with υ = 0.5, G = E/3. In Abaqus, it allows for specifying a table of plastic shear strain γ_p versus mobilized shear stress τ to consider the nonlinear stress-strain material behavior[15]. In this study, the stress-strain responses are calculated using the hardening relation described by (12) and then used as input in Abaqus.

$$\frac{\tau}{S_u} = 2\frac{\sqrt{\gamma^p / \gamma_f^p}}{1+\gamma^p / \gamma_f^p} \tag{12}$$

where: τ is currently mobilized shear stress, S_u is the shear strength of soil, γ^p is the current plastic shear strain, γ_f^r is the plastic shear strain at failure (full mobilization).

For this study, $\gamma_f^r = 0.15$, and the S_u and G value of different layers is shown in Table 3.

Table 1. Geometry and mechanical properties of pile used in FEM analysis.

Pile:	
Length(L)	45 m
Diameter(D)	9 m
Modulus of elasticity of the pile(E)	19.79 Gpa
Poisson's ratio (ν)	0.3

Table 2. Geometry and mechanical properties of sand layer used in FEM analysis.

Sand layer：	
Depth(H)	0-6 m
Submerged unit weight of soil (γ)	10 kN/m3
Reference modulus of elasticity (E)	24 Mpa
Angle of internal friction (φ)	34.25°
Dilation angle (ψ)	4.25°
Cohesion (c)	0
Poisson's ratio (ν)	0.2

Table 3. Geometry and mechanical properties of clay layers used in FEM analysis.

Clay layers:	Dimension	Properties
Clay1	Depth:3-9 m	G=37.56 Mpa su =20 kpa
Clay2	Depth:9-18m	G=70.4 Mpa su =60 kpa
Clay3	Depth:18-36m	G=99.6 Mpa su =120 kpa
Clay4	Depth:36-72m	G=140.8 Mpa su=240 kpa
Clay5	Depth:72-90m	G=215.6 Mpa su =480 kpa

3.2. Contact condition of soil/pile interaction

The Coulomb friction model helps the direction and magnitude of the frictional interface between the outer surfaces of the pile and sand. The friction coefficient (μ) is defined as μ=tan (φμ), where φμ is the pile/soil interface friction angle. The value of φμ depends on surface roughness of the pile and effective angle of internal friction, φ′. Kulhawy (1991) recommended the value of φμ for steel pipe piles in the range of 0.5φ′ ~ 0.9φ′, where lower values are for smooth steel piles. The value of μ=0.3 is used in this study.

4. Model validation

An example is modeled to validate the FEM model. It is set in Yellow River Delta [16], and introduced with physical parameters, step setting, meshing and results test.

4.1. Physical parameters

The model pile is made of steel pipe pile, and a 50mm gap is left between the pile and soil for the grouting of concrete. For the depth of soil layer, 1.25 times the depth of the pile into the soil is used, and the pile with a length of 20 m is used for the model. The soil radius is about 36 times the pile radius. Thus, the influence of boundary effect can be ignored. The model parameters are shown in Table 4.

Table 4. Physical parameters.

Parts	Dimensions	Properties	Interactions
Steel pile	length: 20 m, depth in soil: 15 m outside diameter: 1.1 m thickness: 50 mm	Linear elastic ρ=7800 kg/m3 E = 210 Gpa, ν= 0.3	the top of pile is tied with soil; the outer surface of the pile follows the Mule-coulomb friction law, and the friction coefficient is 0.3; the contact pair adopts finite slip and face to face contact; the radial direction of the side and all the DOFs of the bottom are constrained
Concrete	grouting depth: 15 m thickness: 50 mm	Linear elastic ρ=2500 kg/m3 E=20 Gpa,ν=0.17	
Soil	outside diameter: 40 m depth: 20 m a slot in the center, depth: 15 m diameter: 1.2 m	elastic-plastic, M-C model ρ=1800 kg/m3 E=3 Mpa, ν=0.25 φ=30°ψ=0.1° c=12 kpa	

4.2. Step setting

The displacement control method is adopted for the horizontal loading of the model, and the floating weight of all components was used for calculation. In the real state, it is assumed that the displacement on the seabed mud surface is zero while there is stress in the soil. Thus, the geostress balance must be carried out before the horizontal load is applied: set the density of pile, concrete to consistent with the soil before applying horizontal load, and then apply gravity load to the whole model. The internal stress of soil as the initial condition of the model can be extracted, the gravity is applied to balance the whole geostress field, and then physical load is imposed on pile and concrete to make up the density differences. The experience shows that the geostress calculated by this method is basically consistent with the actual situation.

4.3. Meshing

In ABAQUS, the meshing method and mesh density have a significant impact on the accuracy of analysis results. Because this model involves pile and soil distortion and pile-soil contact analysis, 8-node 6-hexahedral linear reduced integral 3-dimensional solid element (C3D8R) is adopted. It is more suitable for contact analysis, and has a higher accuracy of the displacement analysis. The meshing result is shown in Figure 6.

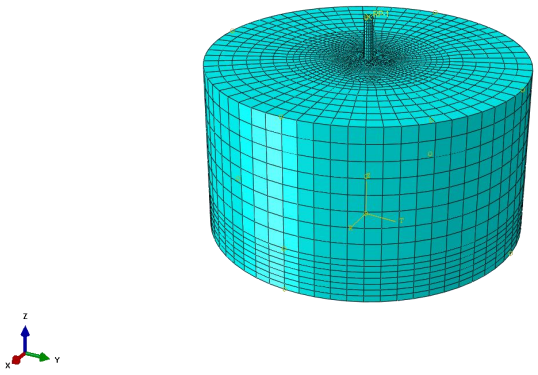

Figure 6. Meshing result.

4.4. Model test

To test the validation of the model, the deflection with the pile is extracted to compare. Displacement of 11.25 cm is applied on the top of the pile, and it is clear that the result matches well with the example in Figure 7. Besides, bending moment with the pile is shown in Figure 8, it can be seen that the test result matches well with the example. The maximum bending moment of the two results occurred at a depth of 3 m, and the difference is about 9 %.

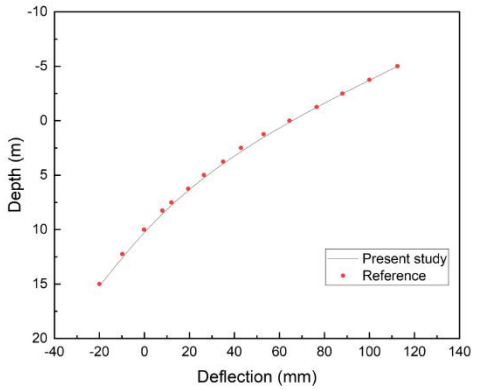

Figure 7. Comparison on deflection with pile.

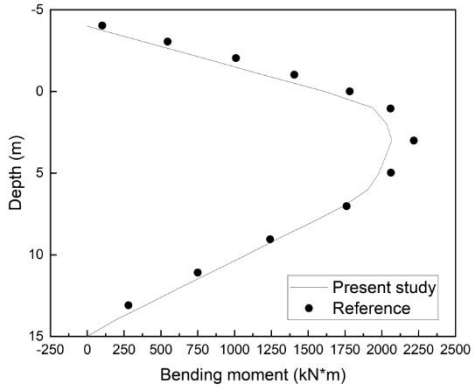

Figure 8. Comparison on bending moment with the pile.

5. Results and discussions

5.1 Convergence verification

To fully consider the accuracy of the results, encryption is made in the area of twice the diameter around the pile. Table 5 shows three types of meshing. After certain force applied on the top of the pile, Figure 9 shows the deflection of the pile of three methods of meshing. It is clear that three methods of meshing match well with other. In view of type A has the shorter computation time and acceptable accuracy, type A is determined.

Type	Encryption	Element number
A	without special encryption	8260
B	encryption on radial direction	16100
C	encryption on radial direction and seabed	17180

Table 5. Types of meshing.

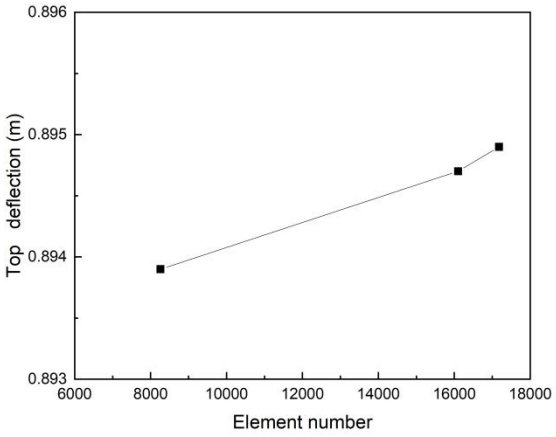

Figure 9. Deflection of three methods of meshing.

5.2. Maximum horizontal displacement

By applying certain displacement on the top surface of the pile, load-deflation curve is presented in Figure 10. It is clear that the reaction has a decreasing growth when displacement exceeds 1.0 m. Thus, several steps are set to get response of different deflation.

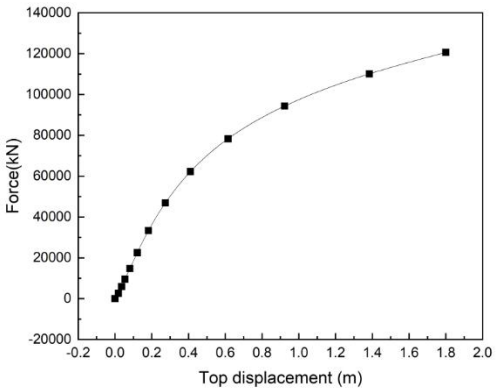

Figure 10. Curve of reaction and displacement of top surface of pile.

5.3. Bending moment with the pile

Figure 11 shows the bending moment with the pile of different displacement. Because of the small flexibility, the whole zone of the pile has bending moment. Figure 11 presents 5 lines to show bending moment of respective displacement. The increase of the displacement of the pile means the increase of the lateral force applied on the top surface. Every increment of the displacement will add a decreasing increment of the maximum bending moment at a depth of 25 m. Under the same horizontal displacement condition of the pile, the bending moment increases gradually from the head, and reached maximum at a depth of 25 m, then decreases with the increase of depth. For different displacement, the maximum bending moment is obtained at a depth of 25 m.

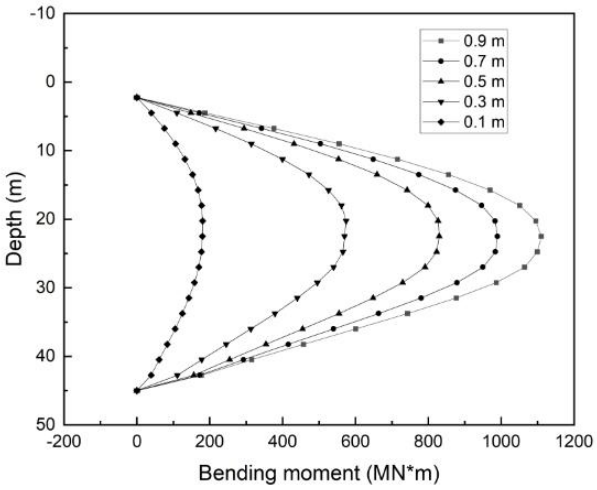

Figure 11. Bending moment of respective lateral displacement.

5.4. Maximum bending moment

Figure 12 shows the variation of the maximum bending moment with lateral displacement. The maximum bending moment increases linearly with increase in lateral load. However, the nonlinearity of the increase is obvious when the displacement exceeds 0.8 m.

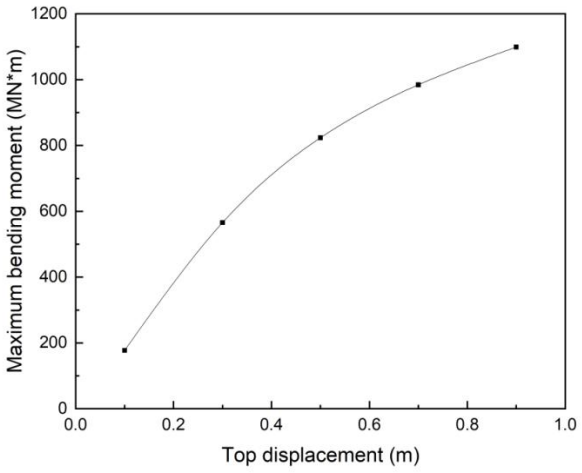

Figure 12. Maximum bending moment with the displacement.

5.5. Lateral displacement of the pile

When the pile is subjected to lateral load, the pile deformation is mainly manifested as horizontal deflection. With the increase of horizontal load, the pile's deflection occurs in the deep zone. Figure 13 shows the deflection of the pile with the depth. With the increase of the displacement, the deflection of the pile increases. The zero deflection point can be calculated by simple interpolation. Table 6 shows the zero point of every displacement, which decreases with the increase of the displacement, the mean value is 40.5 m.

Table 6. Zero point of every displacement.

Displacement of top surface /m	0.1	0.3	0.5	0.7	0.9
Zero displacement coordinate of pile /m	40.85	40.53	40.40	40.38	40.30

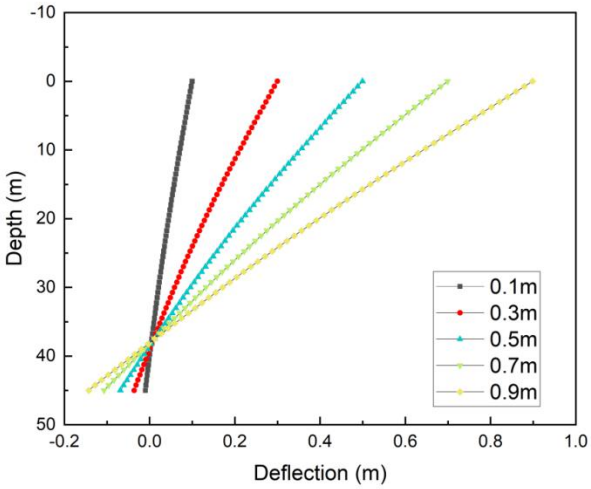

Figure 13. Deflection of the pile.

5.6. Stress with pile

In mechanics of materials, Mises stress is an equivalent stress stemmed from the fourth strength theory. It is commonly used to describe complex stress states under combined action and is the main index to measure the stress level. The calculation formula is:

$$\sigma=\left(\left(\left(\sigma_1-\sigma_2\right)^2+\left(\sigma_1-\sigma_3\right)^2+\left(\sigma_2-\sigma_3\right)^2\right)/2\right)^{\cdots} \quad (12)$$

where σ is mises stress, σ_1 is the first principle stress, σ_2 is the second principle stress, σ_3 is the third principle stress.

The stress nephogram in Figure 14 -17 shows the mises stress with the pile in different displacement. It is clear that, with the increasing of the lateral displacement of the pile top, the stress in the pile in the squeezed side gradually increases from the depth of 20 m below the seabed to the two ends of the pile.

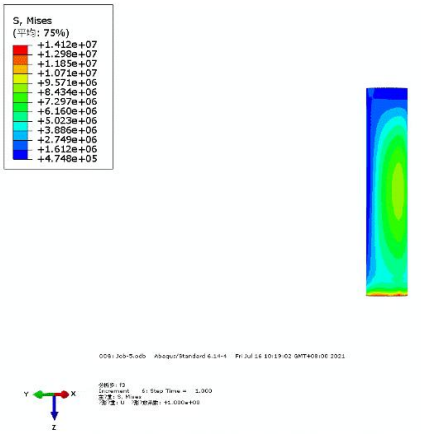

Figure 14. Stress along the pile in the displacement of 0.3 m.

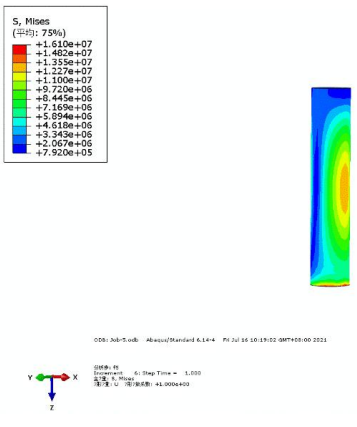

Figure 15. Stress along the pile in the displacement of 0.5 m.

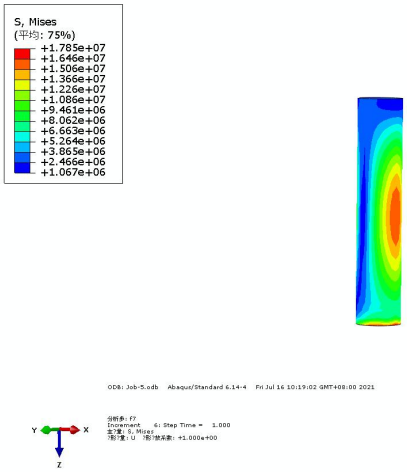

Figure 16. Stress along the pile in the displacement of 0.9 m.

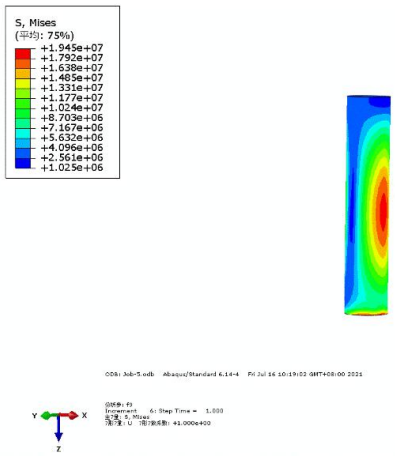

Figure 17. Stress along the pile in the displacement of 0.7 m.

5.7. P-Y Curves

In current engineering practice, nonlinear p-y curves are usually used to simulate load deformation behavior of the soil. In FEM analysis, the soil is modeled as a continuum, not as discrete springs. A group of p-y curves extracted at a depth of 0.75 m, calculated by ABAQUS, API specification and PLAXIS in Figure 18. It shows that the ultimate load from ABAQUS and PLAXIS is generally larger than API specification, while the curve from ABAQUS matches well with PLAXIS. When the displacement exceeds 0.2 m, ultimate reaction from PLAXIS is 12%, larger than that from ABAQUS. Then all the curves show that the soil enters the yield stage, implying the API shows the soil enters the yield stage earlier. As a result, API specification is more conservative than FEM results, no matter it was compared with ABAQUS or PLAXIS. Figure 19-21 show several P-Y curves from several different depth.

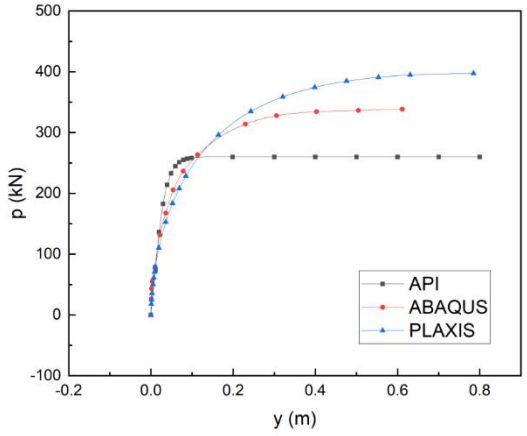

Figure 18. Comparison of p-y curves calculated by three methods at a depth of 0.75 m.

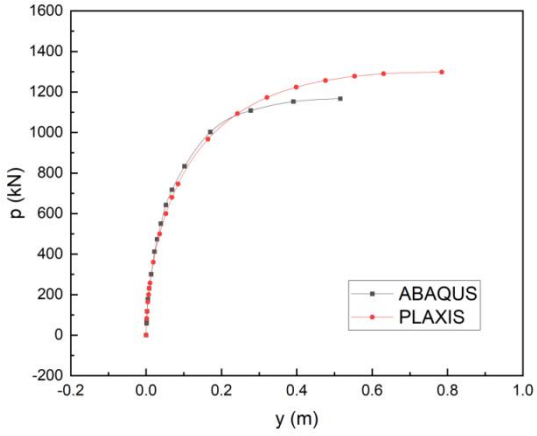

Figure 19. P-Y curves at a depth of 2.25 m.

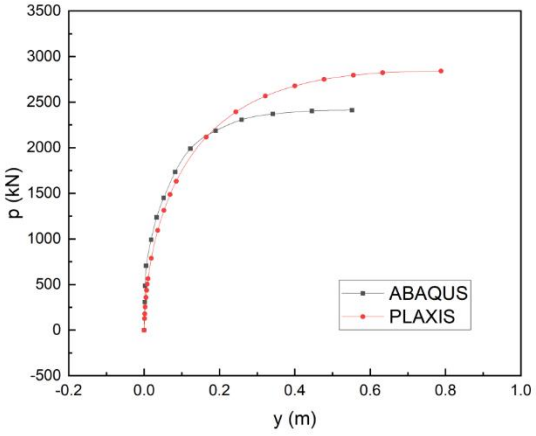

Figure 20. P-Y curves at a depth of 4.5m.

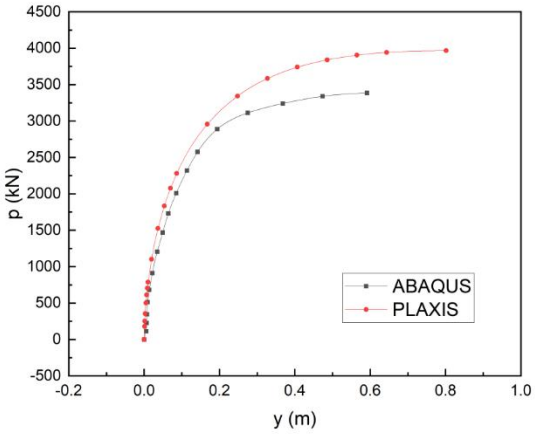

Figure 21. P-Y curves at a depth of 6 m.

5.8. Soil deformation

When the horizontal load is applied near the pile head, the shallow soil first reaches the plastic failure due to its low strength, and then the pile deflection continues to develop to the deeper part, resulting in the deep soil being continuously squeezed by the pile. With the increase of the load, the deep soil also produces plastic yield. Figure 22 clearly shows that the lower part of the pile has a rotation phenomenon. Under the viscous effect of the clay, the displacement of the whole model is mainly the rotation with the bottom of the pile, or in the vicinity location of the soil. Figure 23 presents the area influenced by the lateral load. The whole stress state of the soil is shown in Figure 24.

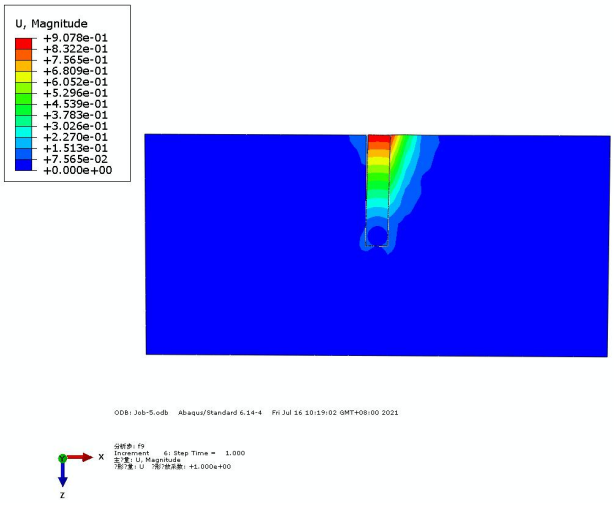

Figure 22. Displacement of the soil.

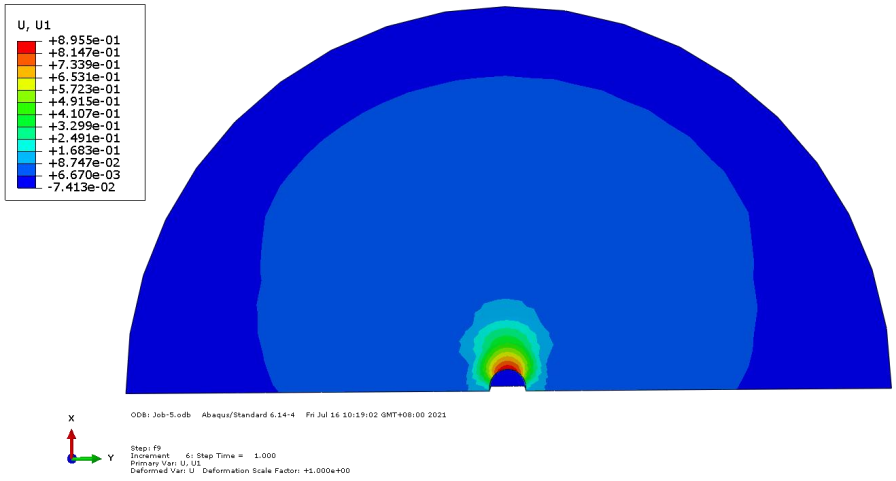

Figure 23. Horizontal displacement U1 contours at the mud surface.

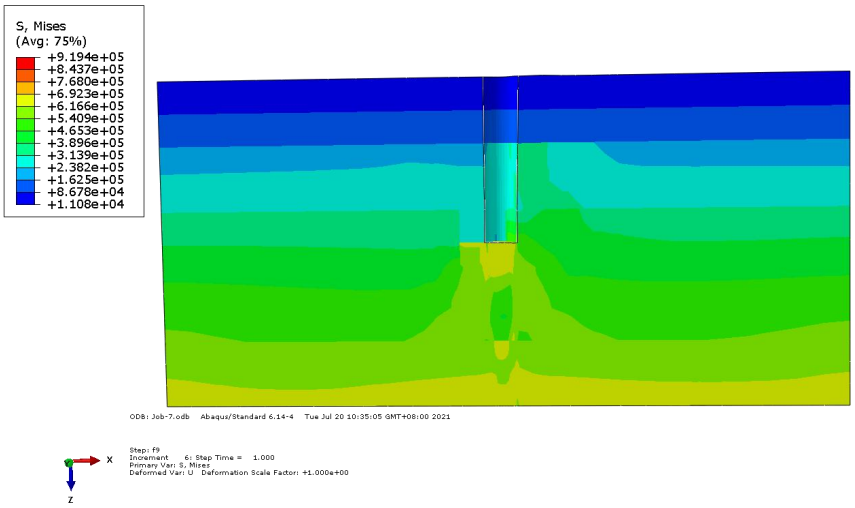

Figure 24. Mises stress of the soil.

6 Conclusions

In the present study, FEM analyses calculated by ABAQUS are performed for a laterally loaded pile with a large diameter in soil. Some mechanical responses with different lateral displacement are presented and the p-y curves are also compared with other methods. In view of this study, the conclusions of this paper are as follows:

●The ultimate displacement of the pile is about 1.0m calculated by displacement controlled method.

●The maximum bending moment exits at a depth of 25m, and a same increment of the depth of 0.2m will generate a decreasing increase.

●The zero-deflection coordinate exist at a depth of about 40.5m, and the value decrease with the increase of the load.

●P-Y curves are given to show the differences of three methods, which presents that the API specification has a more conservative result. However, the results from ABAQUS and PLAXIS matches well before the displacement exceeds 0.2m. The results can be used for reference in the future study and engineering practice.

Author Contributions: Conceptualization, W. S., L. Z., C.M. and X.L.; methodology, W. S., C.M. and X.L.; investigation, J. L., L.Z., W.S. and C.M.; writing—first draft preparation, J. L., L.Z., W.S. and C.M.; review and editing, W. S., C. M. and X. L.; supervision, W. S. and C. M.; project administration, W. S.; funding acquisition, W.S and X.L. All authors have read and agreed to the published version of the manuscript.

Funding: This research was funded by the National Natural Science Foundation of China (Grant No. 52071058, 51939002). This work is also partially supported by Liaoning Revitalization Talents Program (XLYC1807208).

Conflicts of Interest: The authors declare no conflict of interest.

References

[1] Kuo, Y.S.; Achmus, M.; Abdel-Rahman, K. Minimum embedded length of cyclic horizontally loaded monopiles. *J Geotech Geoenviron Eng* **2012**, 138, 357-363.

[2] Alhamaydeh, M.; Barakat, S.; Nassif, O. Optimization of support structures for offshore wind turbines using genetic algorithms with domain-trimming. *Math Probl Eng* **2017**, 2017, 5978375.

[3] Wang, P.; Zhao, M.; Du, X.; Liu, J.;Xu, C. Wind, wave and earthquake responses of offshore wind turbine on monopile foundation in clay. *Soil Dyn Earthq Eng* **2018**, 113, 47-57.

[4] Zheng, X.Y.; Li, H.B.; Rong, W.D.; Li, W. Joint earthquake and wave action on the monopile wind turbine foundation: An experimental study. *Mar Struct* **2015**, 44, 125-141.

[5] Chen, W.Y.; Huang, L.C.; Xu, L.Y.; Zhao, K.; Wang, Z.C.; Jeng, D.S. Numerical study on the frequency response of offshore monopile foundation to seismic excitation. *Comput Geotech* **2021**, 138, 104342.

[6] Caglar, E.; Geoffrey, S. Conceptual sacrificial anode cathodic protection design for offshore wind monopiles. *Ocean Eng* **2021**, 235, 109339.

[7] Klar, A.; Osman, A. S. Load-displacement solutions for piles and shallow foundations based on deformation fields and energy conservation. *Geotechnique* **2008**, 58, 581-589.

[8] Jonkman, J.; Bir, G. Modal dynamics of large wind turbines with different support structure. 27th International Conference on Offshore Mechanics and Arctic Engineering, Estoril, Portugal, 15-20 June 2008.

[9] API. American Petroleum Institute. Recommended Practice for Planning, Design and Constructing Fixed Offshore Platforms - Working Stress Design. Washington D.C. API Publishing Services.2014

[10] Poulos, H. G. Behavior of laterally loaded piles: I - Single pile. *ASCE Soil Mechanics Foundation Division Journal* **1971**, 97, 711-731.

[11] Zhang, J.W.; Liu, H.L.; Dai, Z.H. Study of p-y curve method for computing laterally loaded piles under horizontally distributed loads. *Rock Soil Mech* **2008**, 29, 3370-3374.

[12] Kourkoulis, R.S.; Lekkakis, P.C.; Gelagoti, F.M.; Kaynia, A.M. Suction caisson foundations for offshore wind turbines subjected to wave and earthquake loading: effect of soil–foundation interface. *Geotechnique* **2014**, 64, 171-185.

[13] Cao, G.; Chen, Z.; Wang, C.;Ding, X. Dynamic responses of offshore wind turbine considering soil nonlinearity and wind-wave load combinations. *Ocean Eng* **2020**, 217, 108-155.

[14] Brinkgreve, R.; Engin, E.;Harun Kürat, E. Validation of empirical formulas to derive model parameters for sands. 7th NUMGE, Trondheim, Norway, 3 June 2010.

[15] Zhang, Y.H.;Andersen, K H. Soil reaction curves for monopiles in clay. *Mar Struct* **2019**, 65, 94-113.

[16] Liu, H.J.; Yin, Y.J.;Chang, J.Q. Study of pile-soil interaction of offshore monopile single pile foundation under horizontal load. *Periodical of Ocean University of China* **2016**, 46, 113-120.

[17] Bouzid, D. A. Numerical investigation of large-diameter monopiles in sands: Critical Review and Evaluation of Both API and Newly Proposed p-y Curves. *Int J Geomech* **2018**, 18, 04018441.

[18] Budhu, M.; Davis, T. G. Analysis of laterally loaded piles in soft clays. *J Geotech Eng* **1988**, 114, 21-39.

[19] Thieken et al. Evaluation of p-y approaches for large-diameter monopiles in sand. *Int J Offshore Polar Eng* **2015**, 25, 134-144.

[20] Klaus, T.; Martin, A.; Kirill Alexander, S. On the ultimate limit state design proof for laterally loaded piles. *Geotechnik* **2014**, 37, 19-31.

[21] Negro, V.; López-Gutiérrez, J.; Esteban, M.; Alberdi, P.; Imaz, M.; Serraclara, J.M. Monopiles in offshore wind: Preliminary estimate of main dimensions. *Ocean Eng* **2017**, 133, 253-261.

[22] Zhu, B.T.; Li, W.C.; Yang, M. Static response of monopile to lateral load in overconsolidated dense sand. *J Geotech Geoenviron Eng* **2017**, 143, 1-12.

[23] Luo, R.P.; Yang, M.; L, W.C. Numerical study of diameter effect on accumulated deformation of laterally loaded monopiles in sand. *Eur J Environ Civ Eng* **2020**, 24, 2240-2452.

[24] Lesny, K.; Wiemann, J. Finite-element-modelling of large diameter monopiles for offshore wind energy converters. *American Society of Civil Engineers GeoCongress, Atlanta, United States,* 26 Feb-1 Mar 2006.

[25] Byrne, B. PISA: New design methods for offshore wind turbine monopiles. Offshore Site Investigation Geotechnics 8th International Conference Proceeding **2017**,142-161.